Miner Petrol (2016) 110:125–140
DOI 10.1007/s00710-015-0413-3

ORIGINAL PAPER

Tululite, $Ca_{14}(Fe^{3+},Al)(Al,Zn,Fe^{3+},Si,P,Mn,Mg)_{15}O_{36}$: a new Ca zincate-aluminate from combustion metamorphic marbles, central Jordan

Hani N. Khoury[1] · Ella V. Sokol[2] · Svetlana N. Kokh[2] · Yurii V. Seryotkin[2,3] · Elena N. Nigmatulina[2] · Sergei V. Goryainov[2] · Elena V. Belogub[4] · Ian D. Clark[5]

Received: 5 May 2015 / Accepted: 16 November 2015 / Published online: 27 November 2015

Abstract Tululite ($Ca_{14}(Fe^{3+},Al)(Al,Zn,Fe^{3+},Si,P,Mn,Mg)_{15}O_{36}$ (the hypothetical end-member formula $Ca_{14}\{Fe^{3+}O_6\}[SiO_4][Zn_5Al_9]O_{26}$) (IMA2014-065) is a new natural Ca zincate-aluminate, identified in medium-temperature (800–850 °C) combustion metamorphic (CM) spurrite-fluorellestadite marbles from central Jordan. The type locality (Tulul Al Hammam area) is situated in the northern part of the Siwaqa complex, the largest area of the "Mottled Zone" Formation in the Dead Sea region. The marbles originated from bitumen-rich chalky marine sediments of the Maastrichtian-Paleogene Muwaqqar Chalk Marl Formation, which have low clay content (and, consequently, low Al) and high Zn, Cd, and U enrichments. The bulk CM rocks derived from the low-Al protolith have unusually high (Zn + Cd)/Al ratios (~0.2) and, as a result, a mineralogy with negligibly small percentages of Ca aluminates having low Ca:Al molar ratios (minerals of mayenite supergroup, Ca:Al = 6:7) common to most of calcareous CM rocks in the Mottled Zone. Instead, the mineral assemblage of the Zn-rich marbles contains tululite, with high Ca:Al = 2.55 molar ratios and Zn substituting for a large portion of Al (Zn:Al = 1.1). Tululite occurs in thin clusters as irregular grains with indented outlines (20–100 μm in size), having typical open-work textures associated with rock-forming calcite, fluorellestadite, spurrite, and accessory Zn-rich periclase, lime-monteponite solid solutions, calcium uranates, and zincite. Marbles also bear brownmillerite, dorrite, fluormayenite, high-fluorine Ca aluminate, and lakargiite. Secondary phases are brucite, gel-like calcium silicate hydrates and calcium silicate aluminate hydrates, including Zn- and U-bearing and Cd-rich compounds, Si-bearing hydrated compounds after calcium uranates, and basic Cd chlorides. The empirical formula of the holotype tululite (a mean of 32 analyses) is $(Ca_{13.29}Cd_{0.75})_{\Sigma 14.04}(Al_{5.46}Zn_{5.20}Fe^{3+}_{2.23}Si_{0.95}Mn^{3+}_{1.01}Mg_{0.78}P_{0.41})_{\Sigma 16.04}O_{36}$. Tululite is cubic, space group $F23$; a = 14.9346(4) Å; V = 3331.07(15) Å^3, Z = 4. The strongest lines of the X-ray powder-diffraction pattern [d, Å – (I_{obs})] are: 2.874(57), 2.640 (100), 2.524(42), 2.278(41), 1.760(54), 1.725(25), 1.524(33), 1.500(33). The crystal structure was solved from single-crystal X-ray diffraction data and refined to wR2 = 0.0672 on the basis of 913 unique reflections with $I_0 > 2\sigma(I)$. Tululite belongs to a group of compounds with the general formula $Ca_{14}MT_{15}O_{35+x}$ ($0 \le x \le 1$), and is a new structure type. The tetrahedral framework of tululite structure is formed by T_7O_{13} secondary building units (SBU), which consist of four corner-linked tetrahedra sharing a common oxygen atom and three tetrahedra sharing two O atoms with the neighbor SBU. Ca^{2+} cations occupy three positions; two of them also contain a minor amount of Cd^{2+}. The Ca sites surround an island $(Fe^{3+},Al)O_6$ octahedron and a $(Si,P)O_4$

Editorial handling: L. Bindi

✉ Ella V. Sokol
sokol_ag@mail.ru; sokol@igm.nsc.ru

[1] Department of Geology, The University of Jordan, Amman 11942, Jordan

[2] V.S. Sobolev Institute of Geology and Mineralogy, Siberian Branch of the Russian Academy of Sciences, 3 Koptyug Avenue, Novosibirsk 630090, Russia

[3] Novosibirsk State University, Novosibirsk, 2 Pirogov Street, Novosibirsk 630090, Russia

[4] Institute of Mineralogy UrB RAS, Miass 456317, Russia

[5] Ottawa-Carleton Geoscience Centre, Department of Earth Sciences, University of Ottawa, 140 Louis Pasteur Street, Ottawa, ON K1N 6N5, Canada

tetrahedron in the centers of framework cages at the junction of eight SBUs. The $(Fe^{3+},Al)O_6$ octahedron is coordinated by fourteen Ca positions into a 6-capped cube, whereas the $(Si,P)O_4$ tetrahedron is coordinated by six Ca positions into a regular octahedron. The structural formula of tululite is $Ca_{14}\{Fe^{3+}O_6\}^{M1}[(Si,P)O_4]^{T1}[(Al,Zn)_7O_{13}]_2^{T2\text{-}T4}$. The mineral is yellow with greenish tint, transparent with vitreous luster, non-fluorescent under ultraviolet light, and showing neither parting nor cleavage; Mohs hardness is 6.5. The density calculated on the basis of the empirical formula is 3.826 g/cm^3. Its Raman spectrum shows strong bands at 522, 550 and 636 cm^{-1} and weak bands at 199, 260, 295, 456, and 754 cm^{-1}.

Introduction

The new mineral tululite, $Ca_{14}(Fe^{3+},Al)(Al,Zn,Fe^{3+},Si,P,Mn,Mg)_{15}O_{36}$, $F23$; a = 14.9346(4) Å; V = 3331.07(15) Å^3, (IMA2014-065), was discovered as a relatively abundant accessory phase in phosphorus-rich and trace-element loaded medium-temperature (800–850 °C) combustion metamorphic rocks. The rocks, known under a local name of *varicolored marbles* in central Jordan (Daba-Siwaqa complex of the Mottled Zone), are remarkable for unusual Zn-, Cd-, and U-oxide mineralization (Khoury et al. 2015a, 2015b, 2016). The tululite crystal structure belongs to the structural type of $Ca_{14}MT_{15}O_{35+x}$ ($0 < x \leq 1$) characterized earlier (Abakumov et al. 2005a, 2005b; Grins et al. 2005; Istomin et al. 2007; Kalyuzhnaya et al. 2010) and is the first calcium zincate-aluminate found in natural occurrence. Tululite is the principal concentrator of Al in CM marbles with high (ZnO + CdO)/Al_2O_3 ratios (~0.2), instead of mayenite supergroup minerals (Galuskin et al. 2015a). These natural phases originally described as mayenite ($Ca_{12}Al_{14}O_{33}$) but always containing considerable amounts of F, Cl and/or H_2O are common to many other combustion metamorphic and pyrometamorpic rocks with higher Al contents (Hentschel 1964; Gross 1977; Chesnokov and Bushmakin 1995; Grapes 2011; Sharygin et al. 2013; Galuskin et al. 2015a, 2015b; Sharygin 2015).

The new mineral and its name *tululite* have been approved by the Commission on New Minerals, Nomenclature and Classification, International Mineralogical Association (IMA2014-065) (Khoury et al. 2015b). The name was chosen after the geographical name *Tulul Al Hammam* (Arabic for *Pigeon Hills*) located in the northern Siwaqa area, where the mineral was found. The holotype specimen of tululite is stored in the collection of the Central Siberian Geological Museum of the V.S. Sobolev Institute of Geology and Mineralogy, Novosibirsk, Russia, catalogue number VII-91/1. In this paper we provide details of tululite, report results of its structure determination, and discuss the influence of Zn retention on the mineral assemblages.

Occurrence, rock chemistry, and mineral assemblages

Tululite is a relatively abundant accessory mineral in fine-grained spurrite-fluorellestadite marbles (holotype sample TH-72), medium-temperature (800–850 °C) combustion metamorphic (CM) rocks found in central Jordan. The type locality is situated in the northern Siwaqa area (31°32′N 36°12′E), at a site locally known as Tulul Al Hammam. For details of local geology and rock characterization see (Khoury et al. 2014, 2015a, 2016).

Calcareous CM rocks, mainly spurrite- and fluorapatite/fluorellestadite-bearing marbles, are widespread in central Jordan in the Daba (Khan Az-Zabib) and Siwaqa areas covering more than 1300 km^2 (Khoury and Nassir 1982; Nassir and Khoury 1982; Techer et al. 2006; Khoury et al. 2014, 2015a, 2016). CM marbles were formed by partial decarbonation and sintering of organic-rich calcareous marine sediments of the Maastrichtian-Paleogene Muwaqqar Chalk and Marl Formation, also known as oil-shales, which were deposited at shallow depths in a stable high-productive shelf environment (Zeigler 2001; Abed et al. 2005; Powell and Moh'd 2011; Fleurance et al. 2013; Khoury et al. 2015a). In the Siwaqa area, organic-rich shales were exhumed and exposed to self-ignition and combustion in the Late Quaternary (about 1 Ma years ago). The precursor rocks contain variable amounts of phosphorite and clay and store unusually high contents of P, S, F and trace elements (Cd, U, Ni, Zn, V, Cu, Cr, Ag, Se, Br, I, Sr, and Ba) inherited by the products of metamorphism (Techer et al. 2006; Elie et al. 2007; Fourcade et al. 2007; Abed and Sadaqah 2013; Fleurance et al. 2013; Khoury et al. 2015a). The whole sequence crops out along the valleys (*wadis*), where bituminous chalk and marl are overlain by CM rocks, unconformable Pleistocene travertine, fluvial to lacustrine deposits, and Holocene to Present alluvium. The Tulul Al Hammam varicolored CM marbles typically occur as lenticular bodies from a few meters to more than 60 m thick and form cliffs and hills. Massive marbles are only slightly hydrated while those in fractured and brecciated zones bear signature of heavy secondary alteration.

The area belongs to the Transjordan plateau, a zone of dry climate with a mean annual precipitation of 110 mm, a summer temperature of 44 °C the highest and 23 °C on average, and high evaporation rates. These conditions maintain preservation of many anhydrous (clinker) phases (Khoury et al. 2015a, 2016), including the specific ones typically observed in trace element-loaded cements (Achternbosch et al. 2005; Pomiès et al. 2001; Gineys et al. 2011, 2012) and nuclear waste materials (Golovich et al. 2011).

Primary mineral assemblages

The Tulul Al Hammam marbles are varicolored homogeneous (or rarely foliated), massive, and microcrystalline (up to 50 μm). Numerous 20–100 μm grains of tululite were detected in a typical slightly altered marble sample (#TH-72) containing (in wt%): 4.00 SiO_2, 1.10 Al_2O_3, 0.49 Fe_2O_3, 0.53 MgO, 53.00 CaO, 0.27 Na_2O, <0.05 K_2O, and 3.44 P_2O_5, 1.40 SO_3, and 34.80 LOI. The holotype sample stands out against similar marbles of the same locality in its abnormally high enrichment in Zn (1437 ppm) and Cd (697 ppm). Other trace element concentrations in the sample are elevated but not as high as Cd and Zn: 17 ppm Ag, 579 ppm Cr, 144 ppm Cu, 317 ppm Ni, 7.3 ppm Th, 15.5 ppm U, 211 ppm V, and 31 ppm Zr; Mn is as low as 30 ppm; Co and Sn are <0.4 ppm and <1 ppm, respectively.

The mineral assemblage of TH-72 consists of ~80–85 % calcite, ~7 % fluorellestadite ($Ca_5(SiO_4)_{1.5}(SO_4)_{1.5}F$) – $Ca_5(PO_4)_3F$) segregated into laminas (Fig. 1a), ≤5 vol% Na- and P-bearing spurrite ($Ca_5(SiO_4)_2(CO_3)$), up to 3 vol% of brownmillerite ($Ca_2(Fe_{1-x}Al_x)_2O_5$), and sporadic grains of dorrite ($Ca_2(Mg_2Fe^{3+}_4)(Al_4Si_2O_{20})$). The accessory phases are unevenly distributed in the sample: thin laminas or lenses of fluorellestadite either enclose grains of Zn-, Cd- and Ca-U-oxides or neighbor them at boundaries with calcitic domains.

Tululite is restricted to ~2 mm thick sporadic conformable layers of coarse (up to 100 μm) grains sizes, which contain abundant Zn and Cd (and sometimes U) oxide minerals, minor spurrite and brownmillerite (relative to the bulk rock composition), and no other Ca aluminates (Figs. 1b-f, 3a-c). Tululite coexists with calcite, spurrite, fluorellestadite, Zn-rich periclase (Fig. 2), lime-monteponite solid solution ($(Ca_{1-x}Cd_x)O$) (Khoury et al. 2016) (Fig. 1c), and zincite (very rarely).

Brownmillerite, the main opaque mineral in spurrite-calcite layers, is very scanty in tululite clusters (Figs. 1e,f) and has never been identified enclosed in tululite. Its distribution may be controlled by uneven patterns of authigenic pyrite and clay materials in the sedimentary protolith. In low-Zn spurrite-calcite layers, it is the principal concentrator of Fe^{3+} and Al, as well as Mn (up to 0.2–0.5 wt% MnO) and some Zn (1–3.5 wt% of ZnO). Sporadic small brownmillerites coexisting with tululite are free from Mn and are depleted in Zn (< 1 wt% ZnO).

Outside tululite segregations, there are few <1 to 10 μm isometric grains of two other fluorine-bearing calcaluminates. Fluormayenite ($Ca_{12}Al_{14}O_{32}[\square_4F_2]$), with 46.2–47.8 wt% CaO, 47.4–48.23 wt% Al_2O_3, 0.81–1.55 wt% SiO_2, 0.53–0.85 wt% Fe_2O_3, and 2.12–2.28 wt% F, occurs as few very fine grains in eight thin sections of the holotype sample. The other fluorine-rich Ca aluminate, with 52.22–53.51 wt% CaO, 32.06–34.03 wt% Al_2O_3, 0.64–0.98 wt% SiO_2, 0.77–1.84 wt% Fe_2O_3, and 5.00–5.81 wt% F, is more abundant. All compositions are total deficient (90–92 wt%), i.e., the mineral appears to be hydrated or hydroxylated. We have seen no reports of the natural occurrence of this phase.

Note that the holotype sample bears trace elements (Cd, Ce, Cu, Ni, Th, U, Zn, Zr) accumulated in simple or double oxide accessories: periclase with 20–24 wt% ZnO, 5.0–6.3 wt% NiO, and 2.5–3.4 wt% CuO; an intermediate member of the lime – monteponite solid solution series with 67.1 wt% CdO (on average) and 0.25–0.93 wt% ZnO; zincite with ≤3 wt% CdO; cassiterite; Th-bearing cerianite $(Ce,Th)O_2$, as well as Ti- and U-bearing lakargiite ($Ca(Zr,Ti,U)O_3$). Most of them exist as individual micrometer-sized grains (< 1 to 10 μm). Sample TH-72 also contains unique accessories of high-temperature calcium uranates (Fig. 3a) (Khoury et al. 2015a). Other rare accessories are scanty halite and fluorite.

Secondary mineral assemblages

Sample TH-72 is unevenly hydrated and altered by meteoric water percolated into thin cracks between grains, which is responsible for very low water/solid ratios. Along microcracks, leached spurrite, which has the highest hydraulic reactivity, is converted into porous brownish aggregates of gel-like Ca silicate hydrate (CSH) or Ca silicate aluminate hydrate (CSAH) of a highly variable composition. The common ranges of SiO_2, CaO, and Al_2O_3 in the later are, respectively, 23–31 wt%, 18–34 (occasionally to 4–8 wt%), and 2–6 wt%. The gel-like matter can contain Zn (as 0.5–7 wt% or rarely up to 12–16 wt% ZnO) or U (up to 3.7 wt% UO_3) depending on accessories in the immediate vicinity of altered spurrite grains. Gel-like CSHs and CSAHs aggregates coexisting with tululite and $(Ca_{1-x}Cd_x)O$ grains also store cadmium (3–25 wt%, or rarely to 42–55 wt% CdO). The contents of Ca and Cd are in inverse correlation, which hints to possible existence of compounds intermediate between CSHs with Al and Cd impurities and Cd hydrosilicates with minor Ca. Iron in this gel-like matter is always within 0.1–0.4 wt% or rarely 0.7–1.3 wt% Fe_2O_3, but its content is enough to impart brown tint to the aggregates. Brownish Cd-bearing hydrosilicates are easily spotted by optical microscopy (Figs. 1d-f), but are especially well identified in BSE images. By analogy with the processes discussed by Pomiès et al. (2001), Cd sorption onto the CSH surface or Ca-Cd exchange between precipitated CSHs and Cd-rich chloride solutions appear to be likely candidates as mechanisms of Cd immobilization during supergene alteration of marbles.

Most often periclase is rimmed by brucite, whereas fluorellestadite and brownmillerite remain intact (Figs. 1b-f, 2, 3). Si-bearing hydrated $CaO-UO_3$ compounds commonly form after primary anhydrous Ca-U(VI) oxides (Khoury et al. 2015a). Altered $(Ca_{1-x}Cd_x)O$ grains are surrounded by a halo of Cd and/or Cl-bearing phases, namely basic cadmium chlorides ($Cd(OH)_{2-x}Cl_x$) and fluorite, produced by fluid infiltration along cracks (Khoury et al. 2016). Sometimes the

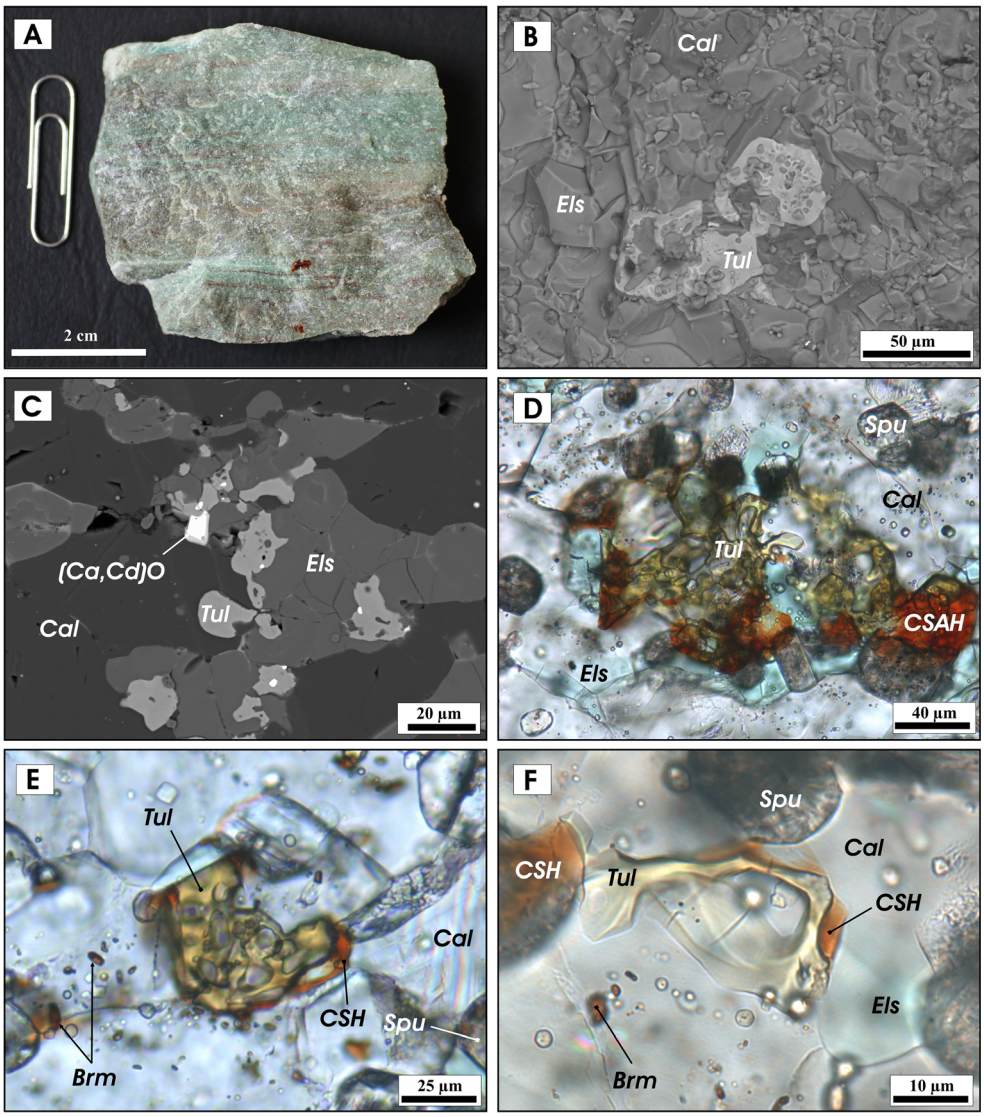

Fig. 1 Morphology of tululite and associated minerals. Holotype sample TH-72. **a** Fragment of spurrite-fluorellestadite marble enriched in tululite. **b,c,d** Typical mineral assemblage of tululite–bearing spurrite marble. Calcite (greyish) and fluorellestadite (turquoise) are rock-forming minerals while spurrite, commonly slightly altered (grey), is of secondary importance. Tululite occurs as open-work grains stuffed with calcite and spurrite inclusions. **e,f** Tululite associated with scanty brownmillerite. BSE images (**b, c**), plane-polarized light (**d, e, f**). *Brm* = brownmillerite, *Cal* = calcite, *CSAH* = Ca silicate aluminate hydrate, *CSH* = Ca silicate hydrate, *Els* = fluorellestadite, *Spu* = spurrite, *Tul* = tululite. (Mineral symbols are according to Whitney and Evans (2010))

assemblage includes also sporadic gains of partially hydrated or hydroxylated chlormayenite ($Ca_{12}Al_{14}O_{32}[\square_4Cl_2]$). Note that tululite bears no signatures of dissolution, substitution or hydration even on contact with hydrated spurrite partially converted to CSHs or CSAHs (Figs. 1d-f). Very thin hydration rims around tululite grains occasionally appear only near open cracks filled with CSHs.

Sample TH-72 stores a whole collection of mineralogical rarities, besides tululite: vorlanite (Galuskin et al. 2011), vapnikite (Galuskin et al. 2014), lakargiite (Galuskin et al. 2008), and fluormayenite (Galuskin et al. 2015a, 2015b) discovered recently in high-temperature calcareous CM rocks of the Hatrurim Fm. and in xenoliths from North Caucasus. There are also some minerals previously unknown in natural occurrence: Cd-rich members of lime-monteponite solid solutions (Khoury et al. 2016), $CaUO_4$ (rhombohedral species, possibly an analog of 'protovorlanite' of Galuskin et al. (2012)) and Ca_2UO_5 (Khoury et al. 2015a), Cd-rich members of $(Ca_{1-x}Cd_x)(OH)_2$ solid solutions and basic cadmium chlorides (Khoury et al. 2016), as well as the fluorine-rich calcium aluminate.

Analytical methods

Holotype marble sample TH-72 was studied by optical thin section petrography, with SEM, EMPA and Raman spectroscopy at the V.S. Sobolev, Institute of Geology and Mineralogy (IGM, Novosibirsk, Russia). Optical properties of tululite were determined at the Institute of Mineralogy UrB RAS in Miass. X-ray diffraction data for the bulk rock sample were collected on a *Philips* powder X-Ray diffractometer with a double goniometer *X'Pert* system (Cu$K\alpha$-radiation with λ = 1.54178 Å) at the Department of Earth Sciences, University of Ottawa. Bulk compositions of major and trace elements were analyzed by atomic emission spectrometry

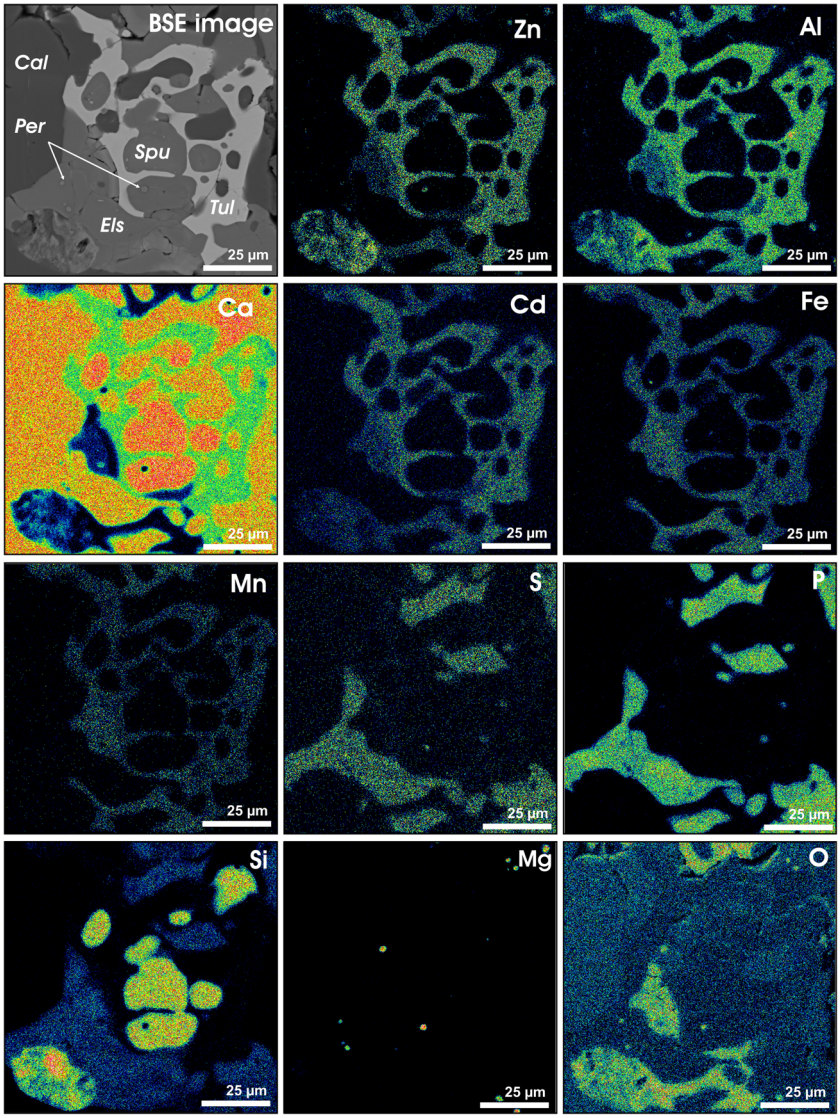

Fig. 2 BSE image and elemental maps for tululite. Holotype sample TH-72. *Cal* = calcite, *Els* = fluorellestadite, *Per* = periclase, *Spu* = spurrite, *Tul* = tululite

with inductively-coupled plasma (ICP-AES) (*IRIS Advantage ThermoJarrell*, Intertechs Corporation, USA) at IGM. The analytical precision was about 10–15 %. Trace-elements in the sample were also analyzed at the Siberian Synchrotron and Terahertz Radiation Centre (SSTRC) at Budker Institute of Nuclear Physics, Novosibirsk, using precise synchrotron radiation X-ray fluorescence analyses (SR XRF) with EDS (energy-dispersion spectroscopy), at 23 kV and 42 kV excitation energies (Phedorin et al. 2000).

Polished thin sections (200–300 µm) were sputter coated with ~30 nm carbon films for EPMA and SEM elemental mapping. Microfabric and phase distribution of samples were assessed on a *JEOL JSM6380LA* scanning electron microscope (IGM) operated at 10 kV and 2.0 nA beam current (measured in Faraday cup), at chamber vacuum pressures of 10^{-5} Torr (~0.01 Pa).

In-situ chemical compositions of individual minerals were analyzed by a JEOL JXA-8100 microprobe, in C-coated polished thin sections, with chamber vacuum kept at 10^{-6} Torr (~0.001 Pa) or better. The instrument was equipped with a single EDS spectrometer and five WDS spectrometers with LiF, PET, or TAP crystals. Mineral chemistry was analyzed at 20 kV and 15–30 nA, with 10 s counts, and a beam diameter of 2 µm. The tululite composition was estimated with reference to natural and synthetic standards: diopside (Ca, Mg), Mn-garnet IGEM (Al, Si, Fe, Mn), fluorapatite (P), $ZnFe_2O_4$ (Zn), CdS (Cd). Peak overlaps for CaK_β-PK_α were automatically compensated by the instrument software, and a matrix correction using the ZAF algorithm (Beckhoff et al. 2006) was applied to raw data prior to recalculation into major oxides. Analytical accuracy was within 2 %-relative for >5 wt% elements, and about 5 %-relative for ≤2 wt% elements (P, Mg).

Raman spectra were recorded on a Horiba Jobin Yvon *LabRAM HR800* spectrometer with a 1024 pixel LN/CCD detector using the 514.5-nm emission line of Ar^+ ion laser

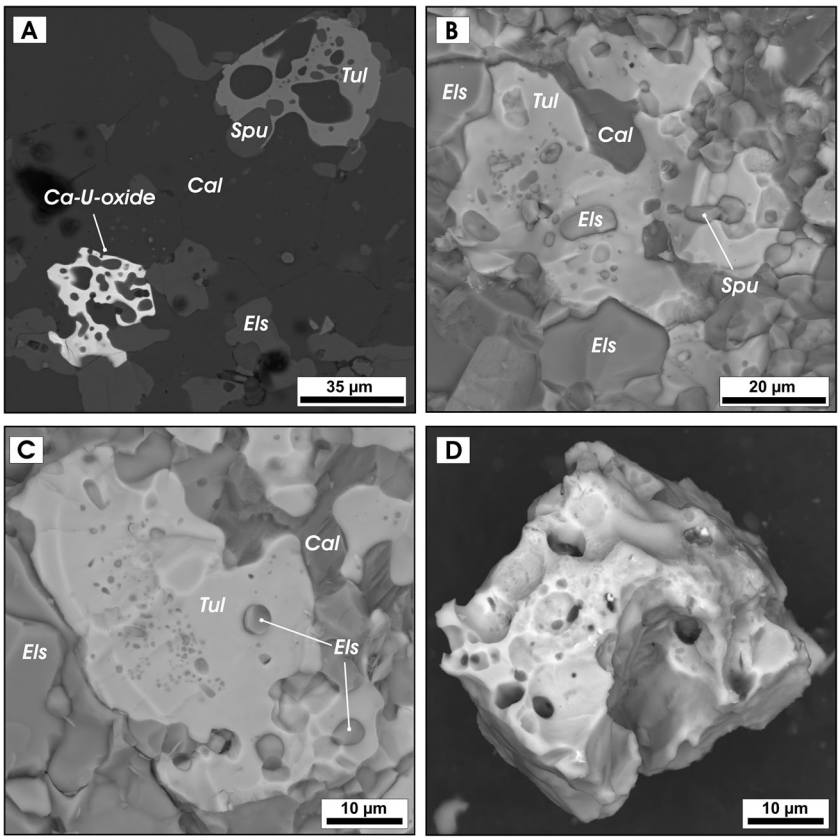

Fig. 3 BSE images show typical morphology of tululite grains stuffed with mineral inclusions. Holotype sample TH-72. **a** Morphology of a tululite grain stuffed with spurrite inclusions and associated with Ca-U(VI) oxide in calcite-fluorellestadite matrix. **b** Fresh tululites stuffed with fluorellestadite, spurrite, and calcite. **c** Small tululite with few fluorellestadite and calcite inclusions. **d** Grain selected for X-ray single crystal structure refinement. *Cal* = calcite, *Els* = fluorellestadite, *Spu* = spurrite, *Tul* = tululite

with the 50 mW maximum beam power (up to 17 mW on the sample surface). The spectra were collected in a back-scattering geometry, using an *Olympus BX41* microscope. For details of instruments and methods see (Goryainov et al. 2012). Spectral resolution of the recorded spectrum Stokes side was set to ~2.2 cm^{-1} at a Raman shift of ~3000 cm^{-1}. The resolution was achieved by using one grating with 1800 grooves/mm and equal 150 μm slit and pin hole sizes. The microscope with an *Olympus PlanLWD 50X* objective lens of the working distance WD = 11 mm with 0.5 numerical aperture provides a focal spot diameter of ~2 μm on the sample surface. The microscope with an *Olympus 50X* objective lens of WD = 0.37 mm with 0.75 numerical aperture for visual spectral range provides the same focal spot diameter (~2 μm). The Raman spectra were deconvolved into Voigt amplitude functions using the *PeakFit* software (Model S506 Interactive Peak Fit 2002).

X-ray experiment

X-ray single-crystal diffraction data were collected on an Oxford *Diffraction Xcalibur Gemini diffractometer* (Mo*Kα* radiation, 0.5 mm collimator, graphite monochromator) at the Novosibirsk State University, Novosibirsk, using a 40 × 40 × 30 μm fragment of optically homogeneous tululite grain free from inclusions (Figs. 3c,d). Data reduction, including background correction and Lorentz and polarization corrections, was performed with the *CrysAlis Pro* software (Oxford Diffraction 2008). A semi-empirical absorption correction was applied using the multi-scan technique.

Least-squares refinement of the position of 913 unique reflections with $I > 2\sigma(I)$ yielded the cubic symmetry: a = 14.9346(4) Å; V = 3331.07(15) $Å^3$, Z = 4. The structure was solved and refined in the space group $F23$ (no. 196) with the SHELX-97 program package (Sheldrick 2008).

The cation distribution at mixed positions was determined with regard to the scattering factors of atoms and their steric features. Minor amounts of Mn^{3+} and Mg^{2+} present in tululite were equally shared between T2 and T3 sites. The occupancies of all mixed cation positions except T1 were refined assuming their full population. In this model, the tululite structure was refined in the anisotropic approximation to wR2 = 11.16 %. Two maximum density values appear in the difference Fourier map: 4.26 e/$Å^3$ (near T2) and 3.49 e/$Å^3$ (near T3). Displacement of trivalent cations from T2 and T3 to the split positions T2' and T3' upon further refinement reduced wR2 down to 6.82 % (Table 1). As a result, however, the O4 position has not been refined with the anisotropic displacement parameters (Table 2). O occupancies were refined as well during the structure refinement. Special attention was given to the O1 and O2 sites because they are partly vacant in some related $Ca_{14}MT_{15}O_{35+x}$ ($0 \le x < 1$) structures (Barbanyagre et al. 1997, Istomin et al. 2007). All six

Table 1 Data collection and structure refinement details for tululite

Chemical formula	$Ca_{13.48}Cd_{0.57}P_{0.42}Mg_{0.82}Si_{0.97}Mn^{3+}_{1.03}Fe^{3+}_{2.42}Zn_{5.76}Al_{4.82}O_{36}$
Space group	*F*23
a (Å)	14.9346(4)
V (Å^3)	3331.07(15)
Z	4
Crystal size (mm)	0.04x0.04x0.03
θ range for data collection	2.36 to 31.82
Index ranges	$-21 \le h \le 21$
	$-22 \le k \le 22$
	$-21 \le l \le 21$
No. of measured reflections	16,871
No. of unique reflections	971
No. of observed reflections ($I > 2\sigma(I)$)	913
No. of parameters refined	63
R_{int}	0.0754
Extinction coefficient	0.00004(2)
Flack parameter	0.14(5)
R1, *wR2* for $I > 2\sigma(I)$	0.0411, 0.0672
R1, *wR2* all data	0.0462, 0.0682
GooF	1.214
Residual electron density (e/Å^3)	0.558, –0.783

independent O positions in the tululite structure were found to be fully occupied, and their occupancies were constrained to be 1.0 in the final cycles of structure refinement.

The results are summarized in tables: Table 1 for final refinement parameters with experimental data; Tables 2 and 3 for coordinates, displacement parameters, and atomic occupancies; Table 4 for bond distances and selected angles.

Powder XRD data for tululite were obtained on a *STOE IPDS 2T* single-crystal diffractometer equipped with an image plate detector (Mo$K\alpha$ radiation; sample-detector distance 120 mm), using the Gandolfi method. The data (Table 5) were processed with *PowderCell* (Nolze and Krause 1998).

Appearance, morphology, physical and optical properties

Tululite exists as 20–100 μm irregular grains with indented outlines or less frequently as roundish grains (Figs. 1b-f, 3). The grains exhibit typical open-work textures with numerous inclusions of calcite and spurrite or rarer flourellestadite or Zn-rich periclase in a tululite matrix (Figs. 1d-f, 2, 3). The total volume of inclusions often reaches or exceeds half of the grain volume. The general pattern is that larger tululites host higher percentages of foreign phases (Figs. 2, 3).

Tululite is yellow with a greenish tint (Figs. 1d-f) and white streaks. It is transparent with a vitreous luster and does not fluoresce under ultraviolet light. Neither cleavage nor parting have been observed. The mineral has irregular brittle fracture. Its Mohs hardness and microhardness are, respectively, 6½ and VHN_{50} = 715–740 kg/mm^2 (a mean of 729 kg/mm^2 (N = 10)). The density could not be measured because of small grain size and numerous inclusions, and was calculated from unit cell size and EMPA data to be 3.826 g cm^{-3}.

Table 2 Atom coordinates, U_{eq} (Å^2) values, and occupancies for tululite

Site	Species, occupation	*x*	*y*	*z*	U_{eq}
Ca1	$Ca_{0.939(8)}Cd_{0.061(8)}$	0.61405(11)	0.61405(11)	0.61405(11)	0.0108(7)
Ca2	$Ca_{0.919(8)}Cd_{0.081(8)}$	0.38739(10)	0.38739(10)	0.38739(10)	0.0072(7)
Ca3	$Ca_{1.00}$	0.21002(7)	0	0	0.0126(3)
M1	$Fe_{0.856(18)}Al_{0.144(18)}$	0.5	0.5	0.5	0.0069(5)
T1	$Si_{0.60}P_{0.40}$	0	0	0	0.0135(7)
T2	$Zn_{0.77}Mg_{0.10}$	0.17169(10)	0.17169(10)	0.17169(10)	0.0165(5)
T2’	$Mn_{0.13}$	0.1451(9)	0.1451(9)	0.1451(9)	0.008(3)
T3	$Zn_{0.639(12)}Mg_{0.10}$	0.82655(18)	0.82655(18)	0.82655(18)	0.0067(7)
T3’	$Mn_{0.13}Al_{0.135(12)}$	0.8425(10)	0.8425(10)	0.8425(10)	0.018(5)
T4	$Al_{0.682(8)}Fe_{0.258(8)}Si_{0.06}$	−0.0010(2)	0.25	0.25	0.0084(3)
O1	1	0.25	0.25	0.25	0.007(3)
O2	1	0.75	0.75	0.75	0.034(5)
O3	1	0.0624(3)	0.0624(3)	0.0624(3)	0.0226(15)
O4	1	0.3709(2)	0	0	0.0091(7)*
O5	1	0.0663(2)	0.3506(2)	0.2541(2)	0.0138(7)
O6	1	0.0664(2)	0.2462(2)	0.8508(2)	0.0148(7)

*O4 position was refined isotropically

Table 3 Anisotropic displacement parameters (Å^2) for tululite

Site	U_{11}	U_{22}	U_{33}	U_{12}	U_{13}	U_{23}
Ca1	0.0108(7)	0.0108(7)	0.0108(7)	−0.0007(5)	−0.0007(5)	−0.0007(5)
Ca2	0.0072(7)	0.0072(7)	0.0072(7)	−0.0016(5)	−0.0016(5)	−0.0016(5)
Ca3	0.0119(5)	0.0136(5)	0.0123(5)	0.000	0.000	−0.0023(12)
M1	0.0069(5)	0.0069(5)	0.0069(5)	0.000	0.000	0.000
T1	0.0135(7)	0.0135(7)	0.0135(7)	0.000	0.000	0.000
T2	0.0165(5)	0.0165(5)	0.0165(5)	0.0005(6)	0.0005(6)	0.0005(6)
T2’	0.008(3)	0.008(3)	0.008(3)	0.006(3)	0.006(3)	0.006(3)
T3	0.0067(7)	0.0067(7)	0.0067(7)	0.0033(6)	0.0033(6)	0.0033(6)
T3’	0.018(5)	0.018(5)	0.018(5)	0.017(6)	0.017(6)	0.017(6)
T4	0.0082(6)	0.0082(6)	0.0089(6)	0.000	0.000	0.0003(4)
O1	0.007(3)	0.007(3)	0.007(3)	0.000	0.000	0.000
O2	0.034(5)	0.034(5)	0.034(5)	0.000	0.000	0.000
O3	0.0226(15)	0.0226(15)	0.0226(15)	−0.0025(16)	−0.0025(16)	−0.0025(16)
O5	0.0181(18)	0.0116(16)	0.0118(16)	−0.0017(13)	0.0049(14)	0.0007(13)
O6	0.0166(17)	0.0139(17)	0.0140(16)	−0.0040(15)	−0.0017(13)	−0.0002(14)

Optical properties were measured with a Bloss spindle stage for the 589 nm wavelength using a gel filter. Tululite is isotropic, with the refraction index n = 1.746 (±0.002).

Table 4 Selected bond lengths (Å) and angles (deg.) for tululite

Ca1–O6(3×)	2.266(4)	Ca2–O5(3×)	2.291(4)
Ca1–O4(3×)	2.419(2)	Ca2–O4(3×)	2.391(2)
mean	2.343	mean	2.341
Ca3–O4	2.403(4)	M1–O4(6×)	1.927(3)
Ca3–O6(2×)	2.498(3)		
Ca3–O5(2×)	2.500(3)	T1–O3(4×)	1.614(7)
Ca3–O3(2×)	2.5685(11)		
mean	2.505		
T2–O5(3×)	1.954(4)	O5–T2–O5(3×)	114.61(9)
T2–O1	2.026(3)	O1–T2–O5(3×)	103.65(12)
mean	1.972		
T2–T2’	0.69(2)		
T2’–O5(3×)	1.912(5)	O5–T2’–O5(3×)	118.6(3)
T2’–O3	2.14(2)	O3–T2’–O5(3×)	96.9(7)
mean	1.969		
T3–O6(3×)	1.966(4)	O6–T3–O6(3×)	113.66(13)
T3–O2	1.980(5)	O2–T3–O6(3×)	104.87(16)
mean	1.970		
T3–T3’	0.41(3)		
T3’–O6(3×)	1.903(4)	O6–T3’–O6(3×)	119.77(13)
T3’–O2	*2.39(3)*	O2–T3’–O6(3×)	*92.7(8)*
T4–O6(2×)	1.796(4)	O5–T4–O5	112.5(3)
T4–O5(2×)	1.808(4)	O5–T4–O6(2×)	110.92(16)
mean	1.802	O5–T4–O6(2×)	104.36(15)
		O6–T4–O6	114.0(3)

The mineral does not show hydraulic properties but dissolves in 1.5 % HCl.

Based on the empirical formula and calculated density, the Gladstone-Dale compatibility index [1 – (Kp/K_C)] (Mandarino 2007) is 0.039 (excellent).

Raman spectroscopy

Raman spectra of tululite show one very strong band at 636 cm^{-1}, two bands of medium intensity 522 cm^{-1} and 550 cm^{-1}, and a set of weak bands at 199, 260, 295, 456, 754, 817, 831 and 934 cm^{-1} (Fig. 4). Generally, the Raman bands of tululite are associated with vibrations of tetrahedral groups, presumably AlO_4, ZnO_4, FeO_4 and SiO_4. Narrow band doublet at 817, 831 cm^{-1} and singlet at 934 cm^{-1} are

Table 5 X-ray powder diffraction data for tululite

hkl	d_{obs} (Å)	I_{rel}	d_{calc} (Å)
115, 333	2.872	57	2.874
044	2.627	100	2.640
244, 006	2.513	42	2.524
335	2.277	41	2.278
066	1.757	54	1.760
555	1.721	25	1.725
448	1.522	33	1.524
339	1.498	33	1.500
377, 159, 519	1.443	8	1.444
666, 2.2.10	1.436	8	1.437
088	1.322	4	1.320
2.2.12, 6.4.10, 4.6.10	1.210	10	1.211

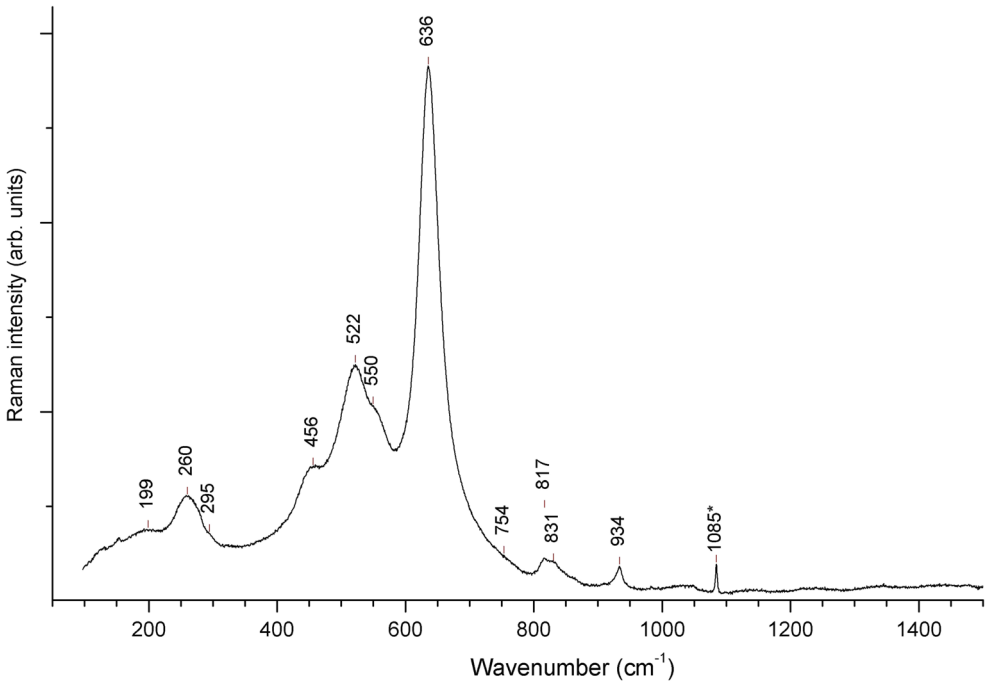

Fig. 4 Raman spectrum of tululite. Holotype sample TH-72

assigned to symmetric ν_1 and antisymmetric ν_3 stretching modes of isolated SiO_4, respectively, at the T1 site.

Broad bands in the range 400 to 760 cm^{-1} correspond to mixed T-O and O-T-O vibrations of tetrahedra at the T2-T4 sites. According to interpretation for mayenite supergroup minerals (Galuskin et al. 2015b), with Al-tetrahedra in their structures, the Raman bands can be attributed to the following vibrations: 200 cm^{-1} to O-Ca-O; 321 cm^{-1} to ν_2 Al-O; 511 cm^{-1} to ν_4 Al-O; 705, 776 cm^{-1} to ν_1 Al-O; and 881 cm^{-1} to ν_3 Al-O. Taking into account this interpretation for AlO_4 vibrations and interconnected tetrahedra and other polyhedra in tululite, we suggest that doublet (522, 550 cm^{-1}) and singlet (636 cm^{-1}) bands correspond, respectively, to mixed vibrations of ν_4 AlO_4 and ν_1 $(Fe^{3+})O_4$ and to dominant vibrations of ν_1 AlO_4. Note that other tetrahedra also contribute to these vibrations due to corner interconnections of tetrahedra, excluding isolated SiO_4 in T1 site.

As inferred by D'Ippolito et al. (2013) for vibrations of gahnite structure, where ZnO_4 tetrahedra and AlO_6 octahedra are available, the bands lower 250 cm^{-1} are due to Zn-O vibrations, whereas the higher frequency band at 661 cm^{-1} is due to motions of oxygen atoms as breathing mode of AlO_6 octahedra of gahnite. Proceeding from this interpretation, supported by calculations of $ZnAl_2O_4$ phonon spectrum (Fang et al. 2002), we attribute the 260 cm^{-1} band in the tululite spectra to dominant contribution of ν_1 ZnO_4 tetrahedra.

In the spectra of complex oxide shulamitite ($Ca_3TiFe^{3+}AlO_8$) reported by Sharygin et al. (2013), modes lower than 400 cm^{-1} represent vibrations of CaO_8 polyhedra and $(Fe^{3+},Ti)O_6$ octahedra, whereas modes in the 450–600 cm^{-1} and 700–900 cm^{-1} ranges are associated with bending and stretching vibrations of $(Al,Fe^{3+})O_4$ tetrahedra, respectively. In tululite octahedra $(Fe^{3+})O_6$, the stretching modes should be located below 400 cm^{-1}, including a wide band at 199 cm^{-1}. We interpret the tululite bands at the 450–900 cm^{-1} range as bending and stretching vibrations of $(Al,Fe^{3+},Si)O_4$ tetrahedra, where the contribution of stretching $(Fe^{3+})O_4$ motions may be considerable at 456, 522 and 550 cm^{-1}.

Bands in the range 100 to 300 cm^{-1}, usually interpreted as lattice modes, have contribution of translational vibrations of cations and rotational and translational vibrations of all tetrahedra and octahedra. Tululite has no bands in the OH stretching region. All spectra contain a weak band at 1085 cm^{-1} due to calcite impurity.

Mineral chemistry

Representative analyses of holotype tululite sample TH-72, with its composition averaged over 32 EMPA analyses (Table 6), show variations in the ranges 37.28 to 41.20 wt% CaO, 20.41 to 25.02 wt% ZnO, 12.31 to 14.55 wt% Al_2O_3, 5.84 to 9.58 wt% Fe_2O_3, 3.76 to 8.54 wt% CdO, 3.53 to 4.29 wt% Mn_2O_3,1.64 to 3.05 wt% SiO_2, 1.45 to 2.29 wt% MgO, 0.70 to 1.89 wt% P_2O_5. Grains from different segregations differ especially in the contents of Zn, Cd, and Fe, but the compositions of individual grains are uniform, with negligible core-to-rim variations. According to Raman spectroscopy, tululite lacks $(OH)^-$ groups and H_2O.

Table 6 Chemical composition of holotype tululite (sample TH-72), Tulul Al Hammam area, central Jordan (wt%)

Sample	LLD	1	s.d.	Range	2	3	4*	5	6
n		32							
SiO_2	0.01	2.96	0.31	1.64–3.05	3.05	2.12	2.99	1.64	2.07
Al_2O_3	0.02	14.50	0.85	12.31–14.55	13.40	15.62	12.67	12.67	13.73
Fe_2O_3	0.02	9.25	1.04	5.84–9.58	7.71	5.84	9.94	9.46	8.39
MgO	0.02	1.64	0.15	1.45–2.29	1.45	1.69	1.70	1.65	1.93
CaO	0.01	38.80	0.85	37.28–41.20	41.20	39.78	38.93	38.02	38.60
ZnO	0.07	22.04	1.08	20.41–25.02	20.41	25.02	24.14	23.44	21.38
CdO	0.07	5.04	1.19	3.76–8.54	6.17	4.95	3.76	7.19	8.54
Mn_2O_3	0.05	4.17	0.14	3.53–4.29	4.01	4.09	4.17	4.24	4.26
P_2O_5	0.02	1.51	0.29	0.70–1.89	1.89	0.70	1.52	1.54	1.23
Total		99.91			99.29	99.81	99.83	99.86	100.12
Formula based on 36 oxygens, apfu									
Si		0.95			0.99	0.69	0.97	0.55	0.68
Al		5.46			5.11	6.00	4.82	4.96	5.33
Fe^{3+}		2.23			1.88	1.43	2.42	2.37	2.08
Mg		0.78			0.70	0.82	0.82	0.82	0.95
Ca		13.29			14.27	13.88	13.48	13.54	13.61
Zn		5.20			4.87	6.02	5.76	5.75	5.20
Cd		0.75			0.93	0.75	0.57	1.12	1.32
Mn		1.01			0.99	1.01	1.03	1.07	1.07
P		0.41			0.52	0.19	0.42	0.43	0.34

n Average of analyses; s.d. standard deviation

*grain selected for X-ray single crystal structure determination

Statistical analysis of 32 representative microprobe analyses reveals significant negative correlations in pairs of oxides, suggesting isomorphic substitutions of elements: CaO – CdO (r^2 = 0.78), Al_2O_3 – Fe_2O_3 (r^2 = 0.71), and MgO – ZnO (r^2 = 0.45).

The empirical formula of tululite based on 36 oxygens (apfu), is $(Ca_{13.29}Cd_{0.75})_{\Sigma 14.04}(Al_{5.46}Zn_{5.20}Fe^{3+}_{2.23}Si_{0.95}Mn^{3+}_{1.01}Mg_{0.78}P_{0.41})_{\Sigma 16.04}O_{36}$. The simplified formula is $Ca_{14}(Fe^{3+},Al)(Al,Zn,Fe^{3+},Si,P,Mn,Mg)_{15}O_{36}$. The structural formula can be expressed as $(Ca_{14}\{Fe^{3+}O_6\}^{M1}[(Si,P)O_4]^{T1}[(Al,Zn)_7O_{13}]_2^{T2\text{-}T4})$. As suggested by Commission on New Minerals, Nomenclature and Classification, International Mineralogical Association (CNMNC IMA), the hypothetical end-member formula of tululite may be represented as $Ca_{14}\{Fe^{3+}O_6\}[SiO_4][Zn_5Al_9]O_{26}$, which requires (in wt%): 43.84 CaO, 22.72 ZnO, 25.62 Al_2O_3, 4.46 Fe_2O_3, 3.36 SiO_2. The real tululite composition obviously differs from the hypothetical end-member in Al deficit (5.5 instead of 9 apfu), compensated by relatively high Zn, Fe, Mn, and Mg.

Crystal structure

In its crystal structure (Fig. 5), tululite has a tetrahedral framework based on T_7O_{13} secondary building units (SBU) (Fig. 6a), which consist of four corner-linked tetrahedra sharing a common oxygen atom (tetrahedral quartet) and three tetrahedra that share two O atoms with the neighbour SBUs and link them to each other (Fig. 6b). The T2 and T3 sites of tetrahedral quartets are occupied by Zn^{2+} and Mg^{2+} (Table 2), with the bond distances between T and O atoms at the group center being larger than other T–O distances (Table 4). The T4 site linking the tetrahedral quartets into a framework is occupied mainly by Al^{3+} and Fe^{3+}, with some amount of Si (Table 2). The T2' and T3' split positions occupied by Mn^{3+} and Al^{3+} are detached from the central O atom (Fig. 6c). An oxygen atom at O3 completes the coordination of T2' to four-fold (Table 4); such a coordination environment is intermediate between tetrahedral and trigonal pyramidal. A long T3'–O2 distance completes the trigonal planar coordination of T3' to a trigonal pyramidal (Table 4). The presence of alternative T' sites apparently leads to a lower coordination number (CN) of central O atoms in tetrahedral quartets but does not change their occupancy.

Ca^{2+} cations occupy three sites; two of them (Ca1 and Ca2) also contain a minor amount of Cd^{2+}. The Ca1 and Ca2 sites are coordinated by six O atoms in a form of a twisted trigonal prism. The coordination of Ca3 site forms a one-capped trigonal prism (CN = 7). The Ca positions surround an island (Fe^{3+}, Al)O_6 octahedron of M1 site and a (Si,P)O_4 tetrahedron of T1

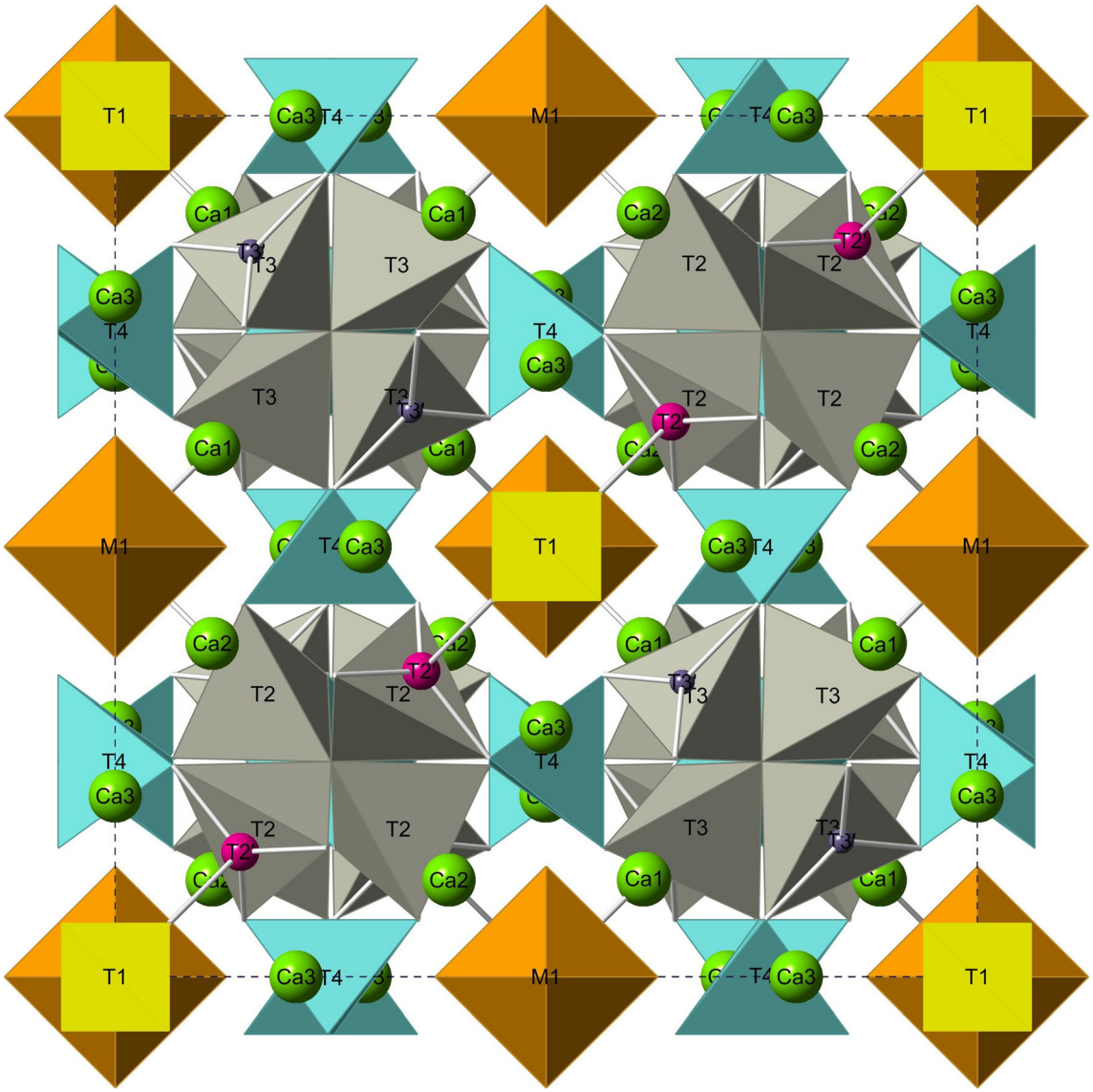

Fig. 5 Tululite structure in (001) projection (see Table 3). Dashed lines show unit cell outlines

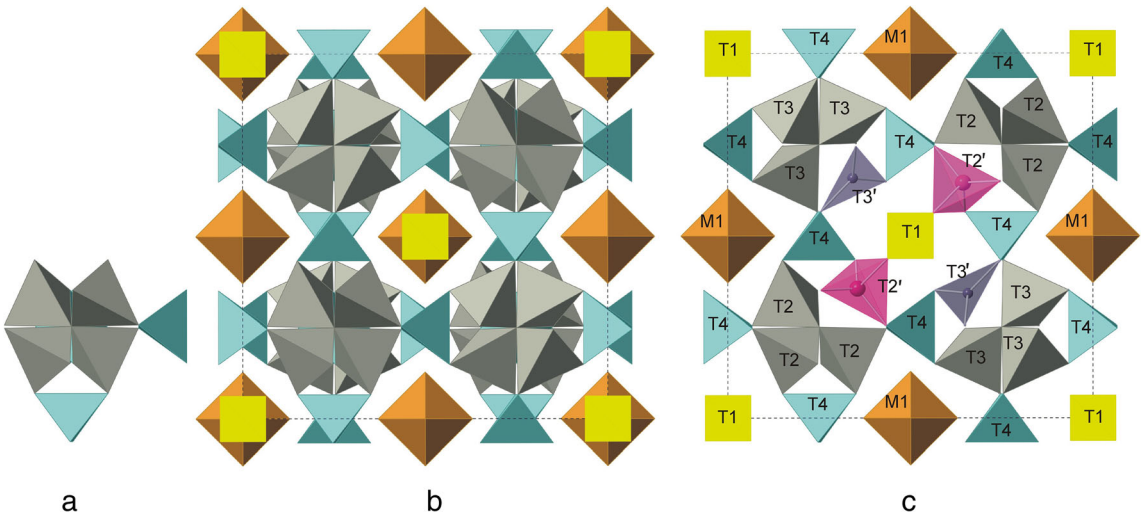

Fig. 6 Secondary building unit (**a**) and their linkage in tululite framework: regular (**b**) and alternative (**c**) distributions of T positions

site, situated in the centers of framework cages at the junction of eight SBUs. The $(Fe^{3+},Al)O_6$ octahedron is coordinated by fourteen Ca positions into a 6-capped cube (Fig. 7a), whereas the $(Si,P)O_4$ tetrahedron is coordinated by six Ca3 positions into a regular octahedron (Fig. 7b).

The reported structure data suggest the mineral to have the final crystal chemical formula $\{(Ca_{13.43}Cd_{0.57})[(Fe^{3+}_{0.86}Al_{0.14})_{M1}O_6]\ [(Si_{0.60}P^{5+}_{0.40})_{T1}O_4]\}\ [(Zn_{5.65}Mn^{3+}_{1.01}Mg_{0.80}Al_{0.54})_{\Sigma 8.00}^{T2-T3}(Al_{4.09}Fe^{3+}_{1.55}Si_{0.36})_{\Sigma 6.00}^{T4}O_{26}]$.

Discussion

Crystal structure and crystal chemistry: comparison with related structures

Tululite apparently belongs to the group of complex oxides with a general crystal-chemical formula $Ca_{14}MT_{15}O_{35+x}$, $0 \le x \le 1$, where M and T are octahedral and tetrahedral sites, respectively, occupied by Al, Zn, Mn, Ga, Co, and Fe (Barbanyagre et al. 1997; Abakumov et al. 2005a; Grins et al. 2005; Istomin et al. 2007; Kalyuzhnaya et al. 2010). All related synthetic compounds have cation sub-lattices as in natural tululite but differ mainly in the distribution of anions.

The $Ca_{14}MT_{15}O_{35+x}$ structure with $x = 0$ is found, for instance, in $Ca_{14}Al_{10}Zn_6O_{35}$ (Barbanyagre et al. 1997), which has the same space group $F23$ as tululite. There are two different tetrahedral groups in $Ca_{14}Al_{10}Zn_6O_{35}$ (Fig. 8): (i) the so-called "ZnS group", similar to tetrahedral quartets that share a common vertex, which is identified in tululite, and (ii) the "cristobalite unit", where the central O site is vacant, and tetrahedra are turned away from the group center (Fig. 8) (Grins et al. 2005). As a result, the $Ca_{14}Al_{10}Zn_6O_{35}$ structure has a single octahedron as an island group, whereas tetrahedra in the cage centers are involved into the framework (note that T1 corresponds to an island tetrahedron in the tululite structure (Fig. 5).

The vacancy at the central O site of the "cristobalite unit" determines oxygen content in the $Ca_{14}Al_{10}Zn_6O_{35}$ compound lower than in tululite.

Note that the structures of non-centrosymmetrical (space group $F23$) $Ca_{14}Al_{10}Zn_6O_{35}$ (Barbanyagre et al. 1997) and tululite are inverted one relative to another, which is evident in different orientations of polyhedra in their projections (see Figs. 5 and 8).

Synthetic compounds $Ca_{14}MT_{15}O_{35+x}$ ($0 < x \le 1$) have higher symmetry (space group $F432$) (Abakumov et al. 2005a; Grins et al. 2005; Istomin et al. 2007; Kalyuzhnaya et al. 2010). As a result, the two types of tetrahedral quartets, as well as their hybrid combinations (Kalyuzhnaya et al. 2010), become statistically distributed throughout the structure.

High symmetry, even at $x = 1$, leads to statistical occupancy of some sites and to appearance of a tetrahedron at the cage center in two statistical orientations (Grins et al. 2005). Note that ordering of two tetrahedral groups in $Ca_{14}MT_{15}O_{35+x}$, at $0 < x < 1$, is impossible within the cubic system, even at lower symmetry. The reason is that the central O position in tetrahedral quartets has the point symmetry 23., and its coordination cannot be less than 4 in the ordered structure.

Thus, ordering in the cubic-system $Ca_{14}MT_{15}O_{35+x}$ compounds is possible only at $x = 0$ and 1 with symmetry not exceeding $F23$. The two ordering possibilities are (i) a structure of the $Ca_{14}Al_{10}Zn_6O_{35}$ type at $x = 0$ (Barbanyagre et al. 1997), and (ii) a structure topologically similar to tululite at $x = 1$. However, no information on synthetic compounds with the $Ca_{14}MT_{15}O_{36}$ tululite structure have been reported to date.

The tululite crystal chemistry is remarkable for $Ca^{2+} \rightarrow Cd^{2+}$ substitution and presence of manganese as Mn^{3+}. Isomorphic substitution $Ca^{2+} \rightarrow Cd^{2+}$, instead of expected $Cd^{2+} \rightarrow Zn^{2+}$, is due to similarity of Cd^{2+} ($r^{[6]} = 0.95$ Å)

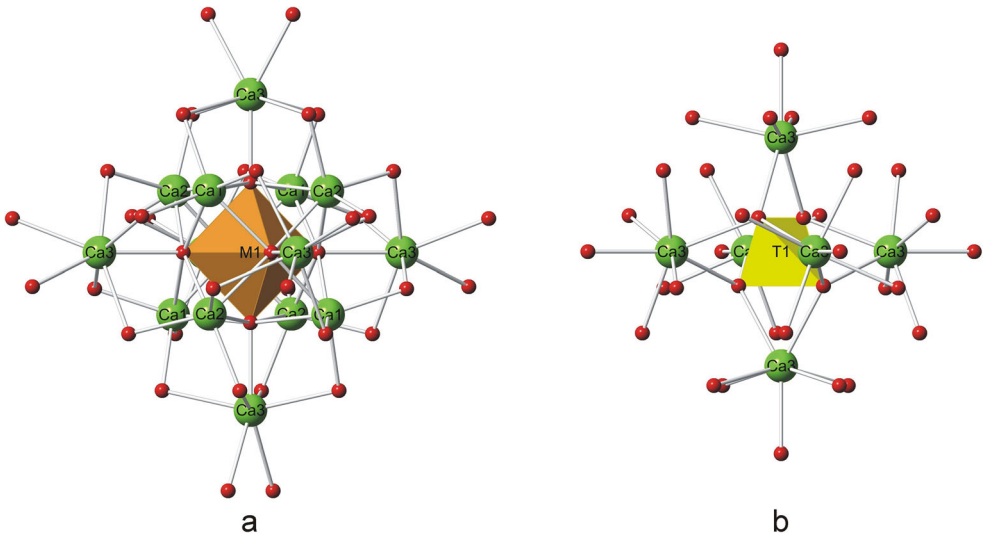

Fig. 7 Island M1 octahedron $(Fe,Al)O_6$ (**a**) and T1 tetrahedron $(Si,P)O_4$ (**b**) with neighboring Ca atoms

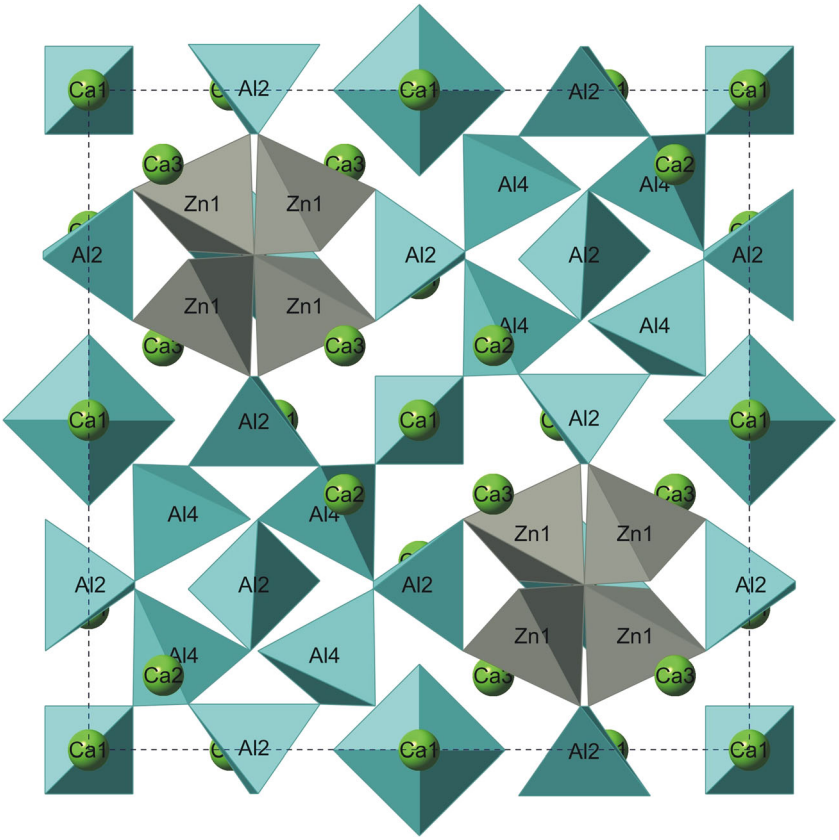

Fig. 8 Structure of $Ca_{14}Al_{10}Zn_6O_{35}$ compound, after (Barbanyagre et al. 1997)

and Ca^{2+} ($r^{[6]}$ = 1.00 Å) ionic radii; it was proven for CaO–CdO solid solutions (Srihari et al. 2011; Khoury et al. 2016). Zn and Cd are inseparable in reducing environments, where they form mixed sulfides (Zn,Cd)S, but diverge in natural oxidizing conditions. Namely, Cd readily becomes separated from Zn and mobilized in the oxidation zone during alteration of Cd-rich sulfide ores, giving rise to smithsonite ($ZnCO_3$) – hemimorphite ($Zn_4(Si_2O_7)(OH)_2{\cdot}H_2O$) ± zincite, hydrozincite ($Zn_5(CO_3)_2(OH)_6$) Zn mineralization and monteponite (CdO) ± otavite ($CdCO_3$) Cd mineralization (De Waele et al. 1999; Schwartz 2000; Ye et al. 2012).

Under the conditions of oxidative sintering, Zn mainly enters zincite and MgO-based solid solutions, while Cd is concentrated in lime-monteponite ($Cd_{1-x}Ca_xO$) solid solutions (Khoury et al. 2016). Both Cd and Zn enter the complex structure of tululite, occupying different sites, with the respective average ratios ($K_{Me} = Me_{mineral}/Me_{rock}$): K_{Cd} = 107.3 and K_{Zn} = 121.4. In tululite Cd^{2+} substitutes for Ca^{2+} in a trigonal prismatic coordination, at average bond distances M–O = 2.34–2.51 Å, whereas Zn^{2+} is present in amounts commensurate with Al^{3+} and occupies the proper tetrahedral sites with an average bond distance of T – O = 1.97 Å.

Manganese valence is a key point in solving the tululite crystal structure and finding its correct formula. The *P-T* parameters of CM alteration of the Tulul Al Hammam marbles fall into the range 600–1000 °C and $p(O_2)$ $1 \div 10^{-2}$ bar, at which Mn_2O_3 instead of MnO is a stable phase in the Mn–O system, as inferred from thermodynamic calculations and experimental data (Stobbe et al. 1999; Grundy et al. 2003). Therefore, Mn is expected to occur in tululite mainly as Mn^{3+}.

Origin of tululite

The Tulul Al Hammam CM marbles were produced by in-situ high-temperature ambient pressure combustion metamorphism of bitumen-rich (C_{org} up to 25 wt%) calcareous marine sediments (mainly chalk) of the Muwaqqar Formation (Fleurance et al. 2013; Khoury et al. 2015a, 2016). The sediments consist mainly of micritic calcite and detritus of planktonic foraminifera shells, with up to 96 vol% $CaCO_3$. The percentages of clay minerals (smectite and illite) are low in most lithologies (0.05 wt% < Al_2O_3 < 3.12 wt%). The sediments contain broadly varying P_2O_5, 3.5 wt% on average, mostly in biogenic carbonate-fluorapatite that occurs as abundant bone detritus and fine irregular nodules. Other constituents are soft clots of radiolarian spicules (consisting of cristobalite opaline matter); bitumen with 8–9 wt% S; and disseminated sulfides (pyrite, Cd-rich würtzite and sphalerite) (Fleurance et al. 2013; Khoury et al. 2016). Thus, the chalky protolith has a major-element composition with high Ca, P, and S, low Si, and very low Al, Fe, Mg, Ti, and alkalis. Judging by relative contents of indicator elements (high P,

Zn, Cd, Ni, Cr, U, V and negligible Co and Mn), the sediments deposited in an upwelling zone acquired abnormal trace element enrichments which were then inherited by the derived CM rocks and gave rise to unique Zn, Cd, U, and Ni accessory mineralization (Techer et al. 2006; Fleurance et al. 2013; Khoury et al. 2015a, 2015b, 2016).

According to the reconstructions by Khoury et al. (2015a, 2016), the Tulul Al Hammam marbles, including the sample TH-72, originated from sediments that underwent near-surface oxidative sintering, accompanied by complete water volatilization. In these conditions, sulfur in sulfides and in sedimentary organic matter oxidizes to higher oxides and partly volatilizes. As a result, abundant (SO_4)-bearing minerals appear in CM marbles, which indicate high oxygen fugacity: fluorellestadite and (SO_4)-rich apatite (Parat et al. 2002; Zateeva et al. 2007; Marks et al. 2012; Kokh et al. 2015). At the same time, all antigenic sulfides (pyrite, würtzite, sphalerite) disappear giving way to oxides (zincite, lime-monteponite solid solution, Zn-, Ni-, Cu-rich periclase) (Khoury et al. 2016) and tululite. Sintering at high oxygen fugacity also produces diverse Ca uranates in CM marbles, with U^{6+} instead of U^{4+} which was originally present in the structure of sedimentary carbonate-fluorapatite (Khoury et al. 2015a).

The tululite-bearing assemblage corresponds to partial decarbonation of chalky matter at ~800–850 °C giving rise to calcite-fluorellestadite-spurrite-brownmillerite, but it lacks higher-temperature Ca silicates such as larnite (Ca_2SiO_4) and/or hatrurite (Ca_3SiO_5). Spurrite marbles bear no signature of melting and should be considered as typical products of solid-state reactions (Reverdatto 1973; Grapes 2011; Khoury et al. 2015a, 2016). The rocks that undergo CM alteration at a temperature below the melting point of their protolith inherit both its chemistry (except for highly volatile compounds) and texture, including uneven distribution of phases that concentrate major and trace elements (Grapes 2011; Sokol et al. 2014).

Sample TH-72 comprises two mineralogically different types of layers. Tululite occurs in the laminas that contain abundant fluorellestadite, oxides of Zn, Cd, Ni, Cu and minor amounts of spurrite and brownmillerite but lack Ca aluminates. To a high probability, they originated from organic-rich chalky sediment rich in phosphorite and disseminated sulfides. Laminas of the other type, being absolutely dominated by calcite and fluorellestadite, also bear spurrite (a Si concentrator), brownmillerite and high-fluorine Ca aluminate (Al concentators). These very laminas contain sporadic fluormayenite grains but are free from tululite.

Such laminar division of primary sediments most likely results from periodic bioproductivity fluctuations. Sediments deposited in periods of high productivity bear S-rich organic matter with high Zn and Cd contents while those corresponding to lower-productivity spans have smaller contents of organic matter being rather rich in clastics and, hence, in Si and Al.

Experiments by Gineys et al. (2011) show that zinc radically modifies the phase assemblages in Portland cement clinkers. Namely, $Ca_6Zn_3Al_4O_{15}$ forms instead of low-aluminium Ca aluminate ($3CaO{\cdot}Al_2O_3$), which decreases at Zn/Al ~ 1, as well as instead of $Ca_3Al_2O_6$, which totally disappears at Zn/Al ~ 1.7. The same effect was reported by Bolio-Arcéo and Glasser (1998, 2000). The Tulul-Am Hammam CM marbles have the (Zn + Cd)/Al ratio approaching 0.2–0.3 in bulk chemistry and reaching 6 in the tululite-bearing layers.

Thus, strong Al deficit, high Zn/Al ratios, local heterogeneity in trace-element loading, and oxidizing thermal treatment of the sedimentary parent rocks below its melting point, produced two assemblages that coexist in CM marbles but differ in number and composition of aluminates. One paragenesis includes tululite as a main Al-bearing phase and brownmillerite as an accessory, whereas the other contains abundant brownmillerite, sporadic high-fluorine Ca aluminate and scanty fluormayenite. Judging by their compositions, tululite competes with fluorine-bearing calcaluminates for Al and with brownmillerite for the limited availability of Fe, Mn, and Al in the protolith.

Thus, the presence of complex zincate-aluminate tululite instead of Al-rich Ca aluminates in the mineral assemblages of Cd- and Zn-rich and Al-depleted CM marbles appears reasonable. Tululite concentrates Cd and Zn which were abundant in the protolith, as well as Mn which was vanishing in the primary sediment and in its metamorphic products (≤ 30 ppm). Average metal incorporation ratios of Cd and Zn are commensurate (K_{Cd} = 107 and K_{Zn} = 121) but differ from average K_{Mn} reaching 500. The tululite structure is remarkable for containing high-valence cations (Si^{4+}, P^{5+}) and strongly oxidized transition elements (Fe^{3+}, Mn^{3+}), which balances the presence of 36 oxygens instead of 35 + x (x < 1) in related synthetic compounds.

Unlike Ca aluminates with high Al:Ca ratios and high hydraulic activity (Taylor 1997), Ca zincate-aluminate tululite is stable in solutions with pH ≥ 7. Its chemical stability allows considering tululite, along with synthetic compound $Ca_6Zn_3Al_4O_{15}$, as efficient Zn and Cd immobilizer for binding hazardous metals in a concrete matrix (Abakumov et al. 2005a; Gineys et al. 2011, 2012). The natural experiment of tululite survival in rocks exposed to supergene environments for about 100 kyr (Khoury et al. 2016) proves long-term Zn and Cd retention by Ca zincate-aluminate phase.

Acknowledgments We wish to thank Prof. Peter A. Williams (University of Western Sidney) for his intellectual contribution to this work. The manuscript profited from editorial efforts by Professor Luca Bindi, Associated Editor of Mineralogy and Petrology and from criticism by two anonymous reviewers. The first author would like to thank the Deanship of Scientific Research at the University of Jordan for the support during his sabbatical year 2012/2013 at the Department of Earth Sciences, University of Ottawa, Canada. Thanks are extended to Late Prof. Andre

Lalonde for his participation in the University of Ottawa collaboration. Thanks are also given to Tara Kell (XRD lab), and Glenn Poirier (Micro-Analysis Lab.) and to Dr. N. Karmanov and M. Khlestov (IGM, Novosibirsk) for assistance during the analytical work. Wadah Faris, Yousef Abu Salheh, and Azzam Azzarah (University of Jordan, Amman) are acknowledged for their help in the field and in preliminary studies. T. Perepelova (IGM, Novosibirsk) is thanked for helpful advice to the present work. Trace element abundances were analyzed by Yu. Kolmogorov at the shared-research Siberian Synchrotron and Terahertz Radiation Centre, Budker Institute of Nuclear Physics (Novosibirsk, Russia). The study was carried out within the limits of Memorandum of Understanding on Academic Cooperation between the the University of Jordan (Amman) and V.S. Sobolev Institute of Geology and Mineralogy SB RAS (Novosibirsk). The Russian contribution was supported by grant 15-05-00760 from the Russian Foundation for Basic Research.

References

Abed AM, Arouri KR, Boreham CJ (2005) Source rock potential of the phosphorite-bituminous chalk-marl sequence in Jordan. Mar Pet Geol 22:413–425

Abed A, Sadaqah R (2013) Enrichment of uranium in the uppermost Al-Hisa phosphorite Formation, Eshidiyya basin, southern Jordan. J Afr Earth Sci 77:31–40

Abakumov AM, Hadermann J, Kalyuzhnaya AS, Rozova MG, Mikheev MG, Van Tendeloo G, Antipov EV (2005a) $Ca_{6.3}Mn_3Ga_{4.4}Al_{1.3}O_{18}$ – A novel complex oxide with 3D tetrahedral framework. J Solid State Chem 178:3137–3144

Abakumov AM, Kalyuzhnaya AS, Rozova MG, Antipov EV, Hadermann J, Van Tendeloo G (2005b) Compositionally induced phase transition in the $Ca_2MnGa_{1-x}Al_xO_5$ solid solutions: Ordering of tetrahedral chains in brownmillerite structure. Solid State Sci 7(7):801–3144

Achternbosch M, Bräutigam KR, Hartlieb N, Kupsch C, Richers U, Stemmermann P (2005) Impact of the use of waste on trace element concentrations in cement and concrete. Waste Manag Res 23:328–337

Barbanyagre VD, Timoshenko TI, Il'inets AM, Shamshurov VM (1997) Calcium aluminozincates of $Ca_xAl_yZn_kO_n$ composition. Powder Diffract 12(1):22–26

Beckhoff B, Kanngießer B, Langhoff N, Wedell R, Wolff H (2006) Handbook of Practical X-Ray Fluorescence Analysis. Springer-Verlag, Berlin, Heidelberg, p 398

Bolio-Arcéo H, Glasser FP (1998) Zinc oxide in cement clinkering: Part 1 system CaO-ZnO-Al_2O_3 and CaO-ZnO-Fe_2O_3. Adv Cem Res 10: 25–32

Bolio-Arcéo H, Glasser FP (2000) Zinc oxide in cement clinkering: part 2 hydration, strength gain and hydrate mineralogy. Adv Cem Res 12: 173–179

Chesnokov BV, Bushmakin AF (1995) New minerals from burned dumps of the Chelyabinsk coal basin (the 8th report). Ural'skii Mineralogicheskii Sbornik 5:3–22(in Russian)

De Waele J, Forti P, Naseddu A (1999) Le "Grotte di Miniera": patrimonio scientifico e risorsa turistica in: Atti del Convegno Internazionale di Studio "Paesaggio Minerario" Cagliari, 7–10 Ottobre 1999; abstracts.

D'Ippolito V, Andreozzi GB, Bosi F, Hålenius U, Mantovani L, Bersani D, Fregola RA (2013) Crystallographic and spectroscopic characterization of a natural Zn-rich spinel approaching the endmember gahnite ($ZnAl_2O_4$) composition. Mineral Mag 77:2941–2953

Elie M, Techer I, Trotignon L, Khoury H, Salameh E, Vandamme D, Boulvais P, Fourcade S (2007) Cementation of kerogen-rich marls by alkaline fluids released during weathering of thermally metamorphosed marly sediments. Part II: Organic matter evolution, magnetic susceptibility and metals (Ti, Cr, Fe) at the Khushaym Matruck natural analogue (central Jordan). Appl Geochem 22: 1311–1328

Fang CM, Loong CK, de Wijs GA, de Wijs G (2002) Phonon spectrum of $ZnAl_2O_4$ spinel from inelastic neutron scattering and first-principles calculations. Phys Rev B66:144301

Fleurance S, Cuney M, Malartre M, Reyx J (2013) Origin of the extreme polymetallic enrichment (Cd, Cr, Mo, Ni, U, V, Zn) of the Late Cretaceous–Early Tertiary Belqa Group, central Jordan. Palaeogeogr Palaeoclimatol Palaeoecol 369:201–219

Fourcade S, Trotignon L, Boulvais P, Techer I, Elie M, Vandamme D, Salameh E, Khoury H (2007) Cementation of kerogen-rich marls by alkaline fluids released during weathering of thermally metamorphosed marly sediments. Part I: Isotopic (C, O) study of the Khushaym Matruk natural analogue (central Jordan). Appl Geochem 22:1293–1310

Galuskin EV, Gazeev VM, Armbruster T, Zadov AE, Galuskina IO, Pertsev NN, Dzierżanowski P, Kadiyski M, Gurbanov AG, Wrzalik R, Winiarski A (2008) Lakargiite $CaZrO_3$: A new mineral of the perovskite group from the North Caucasus, Kabardino-Balkaria, Russia. Am Mineral 93:1903–1910

Galuskin E, Armbrusteter T, Galuskina I, Lazic B, Winiarski A, Gazeeeev V, Dzierżanowski P, Zadov A, Pertsev N, Wrzalik R, Gurbanov A, Janeczek J (2011) Vorlanite $(CaU^{6+})O_4$ – A new mineral from the Upper Chegem caldera, Kabardino-Balkaria, Northern Caucasus, Russia. Am Mineral 96:188–196

Galuskin EV, Galuskina IO, Dubrovinsky LS, Janeczek J (2012) Thermally induced transformation of vorlanite to "protovorlanite": Restoration of cation ordering in self-irradiated $CaUO_4$. Am Mineral 97:1002–1004

Galuskin E, Galuskina I, Kusz J, Armbruster T, Marzec K, Dzierżanowski P, Murashko M (2014) Vapnikite Ca_3UO_6 – a new double-perovskite mineral from pyrometamorphic larnite rocks of the Jabel Harmun, Palestinian Autonomy, Israel. Mineral Mag 78: 571–581

Galuskin EV, Gfeller F, Galuskina IO, Armbruster T, Bailau R, Sharygin VV (2015a) Mayenite supergroup, part I: Recommended nomenclature. Eur J Mineral 27:99–111

Galuskin EV, Gfeller F, Armbruster T, Galuskina IO, Ye V, Dulski M, Murashko M, Dzierżanowski P, Sharygin VV, Krivovichev SV, Wirth R (2015b) Mayenite supergroup, part III: Fluormayenite, $Ca_{12}Al_{14}O_{32}[\square_4F_2]$, and fluor-kyuygenite, $Ca_{12}Al_{14}O_{32}[(H_2O)_4\ F_2]$, two new minerals of mayenite supergroup from pyrometamorphic rock of Hatrurim Complex, South Levant. Eur J Mineral 27:123–136

Gineys N, Aouad G, Sorrentino F, Damidot D (2011) Incorporation of trace elements in Portland cement clinker: Thresholds limits for Cu, Ni, Sn or Zn. Cem Concr Res 41:1177–1184

Gineys N, Aouad G, Sorrentino F, Damidot D (2012) Effect of the clinker composition on the threshold limits for Cu, Sn or Zn. Cem Concr Res 42:1088–1093

Golovich E, Wellman E, Serne R, Bovaird C (2011) Summary of Uranium Solubility Studies in Concrete Waste Forms and Vadose Zone Environments. PNNL-20726, the U.S. Department of Energy, Under Contract DE-AC05, p. 76RL01830

Goryainov SV, Krylov AS, Yu P, Madyukov IA, Smirnov MB, Vtyurin AN (2012) Raman investigation of hydrostatic and nonhydrostatic compressions of OH- and F-apophyllites up to 8 GPa. J Raman Spectrosc 43:439–447

Grapes R (2011) Pyrometamorphism, second edn. Springer, Berlin, p. 290

Grins J, Istomin SYa, Svensson G, Attfield JP, Antipov EV (2005) The disordered cubic structure of $Ca_7Co_3Ga_5O_{18}$. J Solid State Chem 178:2197–2204

Gross S (1977) The mineralogy of the Hatrurim Formation. Israel Geol Surv Israel Bull 70:80

Grundy AN, Hallstedt B, Gauckler LJ (2003) Assessment of the Mn-O system. Basic Appl Res Sec I 24:21–39

Hentschel G (1964) Mayenit, $12CaO{\cdot}7Al_2O_3$, und Brownmillerit, $2CaO{\cdot}(Al,Fe)_2O_3$, zwei neue Minerale in den Kalksteineinschlüssen der Lava des Ettringer Bellerberges. Neu Jb Mineral Mh 1:22–29

Istomin SYa, Chernov SV, Antipov EV, Dobrovolsky YuA (2007) Composition-induced phase transition in $Ca_{14}\ Zn_{6-x}Ga_{10+x}O_{35+x/2}$ (x = 0.0 and 0.5). J Solid State Chem 180(6):1882–1888

Kalyuzhnaya AS, Abakumov AM, Rozova MG, D'Hondt H, Hadermann J, Antipov EV (2010) Synthesis and crystal structure of the new complex oxide $Ca_7Mn_{2.14}Ga_{5.86}O_{17.93}$. Russ Chem B+ 59(4):706–711

Khoury H, Nassir S (1982) A discussion on the origin of Daba – Siwaqa marble. Dirasat 9:55–56

Khoury H, Salameh E, Clark I (2014) Mineralogy and origin of surficial uranium deposits hosted in travertine and calcrete from central Jordan. Appl Geochem 43:49–65

Khoury H, Sokol E, Clark I (2015a) Calcium uranium oxides from Central Jordan: Mineral assemblages, chemistry, and alteration products. Can Mineral 53(1):61–82

Khoury H, Sokol E, Kokh S, Seryotkin Y, Nigmatulina E, Goryainov S, Belogub E, Clark I (2015b) Tululite, IMA2014-065. CNMNC Newsletter No. 23, February 2015, page 53. Mineral Mag 79:51–58

Khoury H, Sokol E, Kokh S, Seryotkin Y, Kozmenko O, Goryainov S, Clark I (2016) Intermediate members of the lime-monteponite solid solutions ($Ca_{1-x}Cd_xO$, x = 0.36–0.55): Discovery in natural occurrence. Am Mineral 101:132–147. doi:10.2138/am-2016-5361

Kokh S, Sokol E, Sharygin V (2015) Ellestadite-group minerals in combustion metamorphic rocks. In: Stracher GB, Prakash A, Sokol EV (eds) Coal and Peat Fires: A global perspective, vol v.3. Elsevier, Amsterdam, pp. 543–562

Mandarino JA (2007) The Gladstone-Dale compatibility of minerals and its use in selecting mineral species for further study. Can Mineral 45: 1307–1324

Marks MAW, Wenzel T, Whitehouse MJ, Loose M, Zack T, Barth M, Worgard L, Krasz V, Eby GN, Stosnach H, Markl G (2012) The volatile inventory (F, Cl, Br, S, C) of magmatic apatite: An integrated analytical approach. Chem Geol 291:241–255

Model S506 Interactive Peak Fit (2002)

Nassir S, Khoury H (1982) Mineralogy, petrology, and origin of Daba-Siwaqa marble, Jordan. Dirasat 9:107–130

Nolze G, Krause W (1998) PowderCell 2.0 for Windows. Powder Diffract 13:256–259

Oxford Diffraction (2008) CrysAlisRED 171.37.35. Oxford Diffraction Ltd, Abingdon, England

Parat F, Dungan MA, Streck MJ (2002) Anhydrite, pyrrhotite, and sulfur-rich apatite: tracing the sulfur evolution of an Oligocene andesite (Eagle Mountain, CO, USA). Lithos 64:63–75

Phedorin MA, Bobrov VA, Chebykin EP, Goldberg EL, Melgunov MS, Filippova SV, Zolotarev KV (2000) Comparison of synchrotron radiation X-ray fluorescence with conventional techniques for the analysis of sedimentary samples. Geostand Geoanal Res 24:205–216

Pomiès MP, Lequeux N, Boch P (2001) Speciation of cadmium in cement: Part I. Cd^{2+} uptake by C-S-H. Cem Concr Res 31:563–569

Powell JH, Moh'd BK (2011) Evolution of Cretaceous to Eocene alluvial and carbonate platform sequences in central and south Jordan. GeoArabia 16:29–82

Reverdatto VV (1973) The facies of contact metamorphism, 262 p. Australian National University Press, Canberra

Schwartz MO (2000) Cadmium in zinc deposits: economic geology of a polluting element. Int Geol Rev 42:445–469

Sharygin VV, Lazic B, Armbruster TM, Murashko MN, Wirth R, Galuskina IO, Galuskin EV, Vapnik Y, Britvin SN, Logvinova AM (2013) Shulamitite $Ca_3TiFe^{3+}AlO_8$ – a new perovskite-related mineral from Hatrurim Basin, Israel. Eur J Mineral 13(25):97–111

Sharygin VV (2015) Mayenite-supergroup minerals from burned dump of the Chelyabinsk Coal Basin. Russ Geol Geophys 56:1603–1621

Sheldrick GM (2008) A short history of SHELX. Acta Crystallogr A64: 112–122

Sokol E, Kokh S, Ye V, Thiéry V, Korzhova S (2014) Natural analogues of belite sulfoaluminate cement clinkers from Negev desert, Israel. Am Mineral 99:1471–1487

Srihari V, Sridharan V, Chandra S, Sastry VS, Sahu HK, Sundar CS (2011) Wide band gap tunability of bulk $Cd_{1-x}Ca_xO$. J Appl Phys 109 (1):013510–1–103510-7

Stobbe ER, de Boer BA, Geus JW (1999) The reduction and oxidation behaviour of manganese oxides. Catal Today 47:161–167

Taylor HFW (1997) Cement Chemistry, second edition, 459 p. Thomas Telford Services, London

Techer I, Khoury H, Salameh E, Rassineux F, Claude C, Clauer N, Pagel M, Lancelot J, Hamelin B, Jacquot E (2006) Propagation of high-alkaline fluids in an argillaceous formation: Case study of the Khushaym Matruk natural analogue (Central Jordan). J Geochem Explor 90:53–67

Whitney DL, Evans BW (2010) Abbreviations for names of rock-forming minerals. Am Mineral 95:185–187

Ye L, Cook NJ, Liu T, Ciobanu CL, Gao W, Yang Y (2012) The Niujiaotang Cd-rich zinc deposit, Duyun, Guizhou province, southwest China: ore genesis and mechanisms of cadmium concentration. Mineral Deposita 47:683–700

Zateeva SN, Sokol EV, Sharygin VV (2007) Specificity of pyrometamorphic minerals of the ellestadite group. Geol Ore Deposit 49(8):792–805

Zeigler M (2001) Late Permian to Holocene paleofacies evolution of the Arabian plate and its hydrocarbon occurrences. GeoArabia 6:445–504